Physics of the Earth and Planetary Interiors 254 (2016) 12–24

Contents lists available at ScienceDirect

Physics of the Earth and Planetary Interiors

journal homepage: www.elsevier.com/locate/pepi

Imaging the inner core under Africa and Europe

J.C.E. Irving

Department of Geosciences, Princeton University, Princeton, NJ, USA

ARTICLE INFO

Article history:
Received 2 November 2015
Received in revised form 1 March 2016
Accepted 3 March 2016
Available online 14 March 2016

Keywords:
Inner core
Anisotropy
PKPdf
Hemisphere boundary

ABSTRACT

The inner core under Africa is thought to be a region where the nature of inner core texture changes: from the strongly anisotropic 'western' part of the inner core to the weakly anisotropic, or isotropic 'eastern' part of the inner core. Additionally, observations of a difference in isotropic velocity between the two hemispheres have been made. A very large new dataset of simultaneous PKPdf and PKPbc observations, on which differential travel times have been measured, is used to examine the upper 360 km of the inner core under Europe, Africa and the surrounding oceans. Inversion of the differential travel time data for laterally varying inner core anisotropy reveals that inner core anisotropy is stronger under central Africa and the Atlantic Ocean than under the western Indian Ocean. No hemispherical pattern is present in Voigt isotropic velocities, indicating that the variation in anisotropy is due to differing degrees of crystal alignment in the inner core, not material differences. When anisotropy is permitted to change with depth, the upper east-most part of the study region shows weaker anisotropy than the central and western regions. When depth dependence in the inner core is neglected the hemisphere boundary is better represented as a line at 40°E than one at 10°E, however, it is apparent that the variation of anisotropy as a function of depth means that one line of longitude cannot truly separate the more and less anisotropic regions of the inner core. The anisotropy observed in the part of the inner core under Africa which lies in the 'western' hemisphere is much weaker than that under central America, showing that the western hemisphere is not uniformly anisotropic. As the region of low anisotropy spans a significant depth extent, it is likely that heterogeneous heat fluxes in the core, which may cause variations in inner core anisotropy, have persisted for several hundred million years.

1. Introduction

Seismic anisotropy in the inner core causes variation in body wave travel times (Morelli et al., 1986; Shearer and Toy, 1991; Creager, 1992; Song and Helmberger, 1995) and body wave attenuation (Souriau and Romanowicz, 1996; Cormier et al., 1998) as well as normal mode splitting functions (Woodhouse et al., 1986; Tromp, 1993; Ishii et al., 2002a; Beghein and Trampert, 2003) and spectra (Durek and Romanowicz, 1999; Irving et al., 2008). In addition to the presence of inner core anisotropy, a 'hemispherical pattern' has been detected using body wave observations of the inner core, where the 'eastern' and 'western' parts of the inner core have differing isotropic velocities, strength of anisotropy and attenuation (for example Tanaka and Hamaguchi, 1997; Creager, 1999; Garcia, 2002a; Oreshin and Vinnik, 2004; Yu and Wen, 2006b; Sun and Song, 2008; Lythgoe et al., 2014). The presence of hemispherical structure in the inner core has not been supported by all investigations, with the influence of mantle structure on travel time observations (Bréger et al., 1999; Bréger et al., 2000; Ishii et al., 2002b), possible structure in the outer core's tangent cylinder (Romanowicz et al., 2003) and both a complex lower mantle and inner core (Tkalčić, 2010) all having been put forward as alternative causes for the observed travel time anomalies. A second, supporting line of evidence for hemispherical inner core structure comes from Earth's normal mode oscillations. Normal modes are sensitive hemispherical anisotropic structure in the inner core (Irving et al., 2009) and observations of coupled normal modes (Deuss et al., 2010) support the presence of distinct eastern and western hemispheres in the inner core. In the western hemisphere, possibly below an uppermost isotropic layer, the presence of anisotropy causes polar rays, which travel close to parallel to Earth's rotational axis, to experience higher velocities than equatorial rays, which travel close to parallel to Earth's equatorial plane. Conversely below the uppermost isotropic layer the eastern hemisphere continues to be isotropic (e.g. Tanaka and Hamaguchi, 1997; Garcia and Souriau, 2000) or displays only weak seismic anisotropy (for example Creager (1999) and Leykam et al. (2010)).

Despite the growing consensus that anisotropy in the inner core is laterally varying, the nature of the transition region between two

E-mail address: jirving@princeton.edu

http://dx.doi.org/10.1016/j.pepi.2016.03.001
0031-9201/

hemispheres is poorly understood. A sharp boundary between two regions with different isotropic velocities was imaged by Waszek et al. (2011), which is not easy to reconcile with some models of inner core dynamics and mineral physics (Geballe et al., 2013). The inner core under Africa is likely to host one of the two boundary region between the two hemispheres. Hemisphere boundaries are normally modeled as a line of constant longitude, though there is some evidence that approximation is too simplistic, at least for the boundary under the Pacific Ocean (Miller et al., 2013; Irving and Deuss, 2015).

A range of locations have been proposed for the boundary between the two hemispheres under Africa (Fig. 1) using observations of several different core-sensitive seismic phases (Fig. 2). Tanaka and Hamaguchi (1997), in the first study of the hemispherical pattern of the inner core, defined the boundaries after expanding the differential travel time residuals of equatorial paths using spherical harmonics. Creager (1999) inspected PKPbc–PKPdf and PKPab-PKPdf differential travel time residuals and found hemisphere boundaries which separated small and large traveltime anomalies for polar paths.

Best-fitting boundaries were located by Irving and Deuss (2011) by systematically seeking the boundary locations which gave the lowest residual error when fitting independent eastern and western hemisphere anisotropy curves to a global dataset of PKPbc–PKPdf and PKPab–PKPdf differential travel times. In a similar way, Lythgoe et al. (2014) used data from absolute PKPdf travel times to find the hemisphere boundary location. As that study contained many rays turning within 550 km of the center of the inner core in addition to rays turning higher in the inner core, their location should be regarded as an average across the entire inner core radius. Modeling the inner core as an anisotropic central body overlain by an isotropic layer of varying thickness, Garcia and Souriau (2000) used absolute PKPdf and PKPbc–PKPdf differential travel times to find the edges of a deeper isotropic region in the inner core. In the resulting eastern hemisphere, an isotropic layer may extend up to 400 km below the inner core boundary (ICB). Miller et al. (2013) selected a preferred boundary location on the basis of forward modeling of equatorial PKPbc–PKPdf seismic data.

A number of other studies have used alternative phases or techniques to seek the hemisphere boundary locations. Several studies used the seismic phase pair of PKPdf and PKiKP to locate the boundary (Niu and Wen, 2001; Wen and Niu, 2002; Garcia, 2002a). The same phase pair has also been used to find independent hemisphere boundaries for three different depth layers in the upper 106 km of the inner core (Waszek and Deuss, 2011).

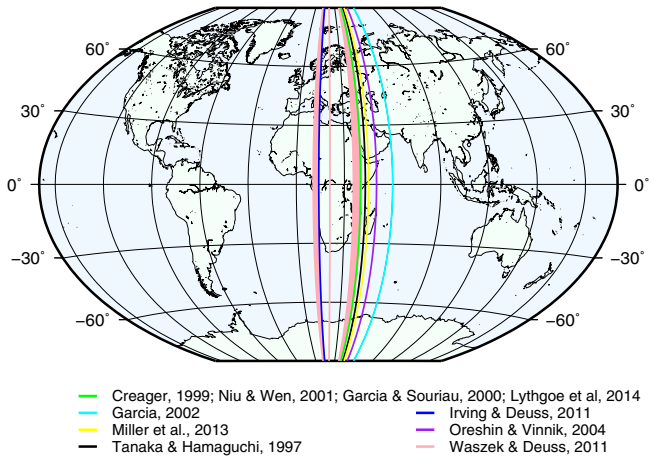

Fig. 1. Locations proposed for the boundary between the 'western' (left) and 'eastern' (right) hemispheres under Africa.

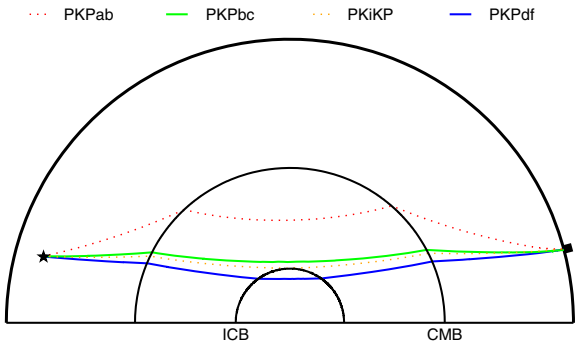

Fig. 2. Raypaths for phases PKPdf and PKPbc (solid lines), which are used in this study, as well as PKiKP and PKPab (dotted lines). Paths are shown those generated by an earthquake at depth of 600 km (black star) traveling to a seismometer at an epicentral distance of 150° (black box).

The hemisphere boundary locations shift eastwards as a function of depth over this relatively small depth range. Differences in the degree of attenuation of PKPdf between the two hemispheres was investigated by Oreshin and Vinnik (2004), who sampled the inner core to a depth of 850 km below the ICB. They found that attenuation in the western hemisphere is anisotropic but isotropic in the eastern hemisphere. As with Lythgoe et al. (2014) the large range of inner core turning depths mean that this boundary should be treated as an average over the upper two thirds of the inner core's radius.

It is likely then, based on multiple studies, that one of the two inner core hemisphere boundaries is located somewhere under Africa, with the modal reported location at 40°E. Some depth variation of the hemisphere boundary is possible, whether it is a true shift in boundary location (Waszek et al., 2011), a change in isotropic layer thickness (e.g. Garcia and Souriau, 2000) or a step-shaped velocity anomaly for equatorial paths (Miller et al., 2013). The inner core translation models of Alboussiere et al. (2010) and Monnereau et al. (2010) would suggest a smooth change in isotropic velocity between the two hemispheres, though the implications of those models for inner core anisotropy are more difficult to predict. Here, a very large new dataset is used to image the isotropic and anisotropic velocity structure under this region to better understand the properties of the inner core close to the transition between the two hemispheres.

2. Data and methods

2.1. Data

PKPbc–PKPdf differential travel times are used to investigate velocity variations in the inner core. PKPdf is a compressional body wave which travels from an earthquake, through the mantle, outer core and inner core. PKPbc takes a similar path, but reaches its deepest point in the outer core (Fig. 2) and arrives several seconds after PKPdf. Using PKPbc–PKPdf differential travel times negates much of the effect of upper mantle structure and earthquake mis-location as PKPdf and PKPbc travel through very similar paths in the shallow Earth, are generated by the same source and recorded at the same station.

Seismograms recorded after selected earthquakes between the beginning of January 1998 to the end of February 2015 were collected from the IRIS DMC (Incorporated Research Institutions for Seismology Data Management Center); for some events these were supplemented by data from the ODC (Observatories and Research Facilities for European Seismology Data Center). The inner core under Africa and surrounding areas is the target of this study. Thus,

only seismograms corresponding to PKPdf raypaths which turn in the inner core between 30°W and 60°E are analyzed here. The events used (Supplementary Table ST5) have source depths ranging from 4–649 km.

Seismograms were de-trended and had their mean and instrument responses removed, leaving the dependent variable as velocity, and were then filtered using a 0.5–1.5 Hz bandpass filter. Suitable maxima or minima corresponding to the PKPdf and PKPbc arrivals are hand-picked on each seismogram (using the Seismic Analysis Code, SAC, Goldstein et al., 2003). All seismograms used have a signal-to-noise level of two or more, where the signal amplitude corresponds to the PKPdf arrival and the noise is the highest amplitude in the time window which starts 30.0 s and ends 2.0 s before the PKPdf pick. Waveforms where the PKPdf and PKPbc arrivals could not be confidently selected were not used. Hand picking of PKPdf and PKPbc (or PKiKP) maxima or minima has been carried out by a range of studies (for example Isse and Nakanishi, 2002; Irving and Deuss, 2015; Miller et al., 2013; Ovtchinnikov et al., 2012; Yu et al., 2005). A number of studies have shown that hand picking gives results very similar to picking individual maxima (or minima in the case of PKiKP), whether for differential travel times (Cao and Romanowicz, 2004; Creager, 1997; Yu and Wen, 2006a; Ohtaki et al., 2012), or for the differences between differential travel times (Mäkinen and Deuss, 2011; Yu, 2016). The sampling rates of the seismograms used are nearly all 0.05 s or below; 33 seismograms have sampling rates of 0.1 s^{-1}. Thus the errors on the differential travel times are expected to be roughly 0.1 s or less. Differential travel time errors, comprising picking errors together with errors caused by source mis-location and heterogeneous Earth structure are assumed to be randomly distributed when the data is inverted; each datum is assigned the same weight in the inversion (Section 2.2).

Event move-out plots, showing all the seismograms for one event, were created for each event to check for waveform similarity and minimize the risk of cycle-skipping. Synthetics seismograms were calculated for each event using the wkbj method (Chapman, 1978; Chapman and Orcutt, 1985) and the CMT focal mechanism for each event (see Dziewonski et al., 1981; Ekström et al., 2012 and globalcmt.org); record sections of these synthetic seismograms were treated in the same way as the data and visually inspected for any potential changes in polarity between the PKPdf and PKPbc arrivals given the strike, dip and slip of the reported earthquake mechanism. To avoid oversampling one region of the inner core with one event, the seismograms used in this study from an individual earthquake (or same-day aftershocks) were not permitted to have both the same epicentral distance and ray angle in the inner core to one and two decimal places. The practical effect of this requirement was that some records from very tightly clustered arrays and temporary networks were not used. An example of the waveform data used, corresponding to one earthquake, is shown in Fig. 3.

Where possible the times and locations of the earthquakes were gathered from the EHB catalog (Engdahl et al., 1998); where this was not possible the PDE catalog [as distributed by globalcmt.org] was used. Estimates of corrections due to ellipticity of the Earth (Dziewonski and Gilbert, 1976) for both PKPbc and PKPdf were calculated [using the ttimel software of Kennett and Gudmundsson (1996) and the published version of Earth model ak135, Kennett et al. (1995)] and used to calculate an ellipticity correction for every seismogram. Ellipticity corrections for differential travel times are very small, ranging from −0.09 to 0.06 s.

Ray angle, ζ, describes the angle between a ray in the inner core and Earth's rotation axis (e.g. Eq. (2) of Irving and Deuss (2011)); a single, constant, value for ζ is used for each ray. Inner core anisotropy causes rays with small ζ to travel through the inner core

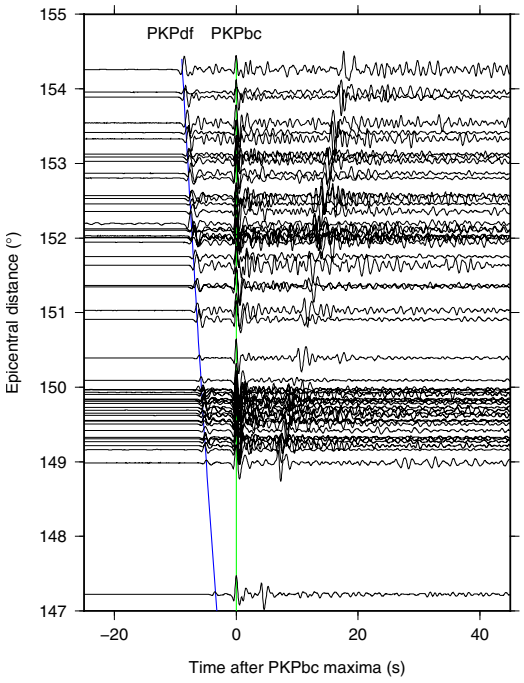

Fig. 3. Waveforms used for event evt20070721 (8.110°S, 71.246°W, depth = 635 km) recorded at stations in Asia shown as a function of epicentral distance. Seismograms are aligned on the observed PKPbc maxima (green line) and have been normalized to the same maximum amplitude in the window from 30 s before the PKPdf arrival to 70 s after the PKPdf arrival for the purposes of display. The blue curve indicates ak135 predictions for the PKPdf arrival times. Differential travel time residuals for these seismograms vary from −0.47 s to +0.55 s after ellipticity corrections. The arrival following PKPbc and moving out with increasing epicentral distance is PKPab. (For interpretation of the references to color in this figure legend, the reader is referred to the web version of this article.)

more quickly than those with large ζ. The fractional velocity perturbation, $\delta v/v$ due to inner core anisotropy is represented by:

$$\frac{\delta v}{v}(\zeta) = a + e\cos(2\zeta) + f\cos(4\zeta) \tag{1}$$

where a, e and f are dimensionless parameters. This form of the anisotropy equation (used by, for example Shearer et al. (1988) and Song and Helmberger (1993)) is equivalent to versions used by other authors (e.g. Creager, 1999; Garcia and Souriau, 2000; Sun and Song, 2008; Lythgoe et al., 2014); this version is chosen so that the ζ dependent terms, by which a, e and f are multiplied, are orthogonal over the range $0 \leqslant \zeta \leqslant 90$. The values of a, e and f may vary radially and laterally if the inner core is not homogeneous.

The strength of inner core anisotropy is normally described as the difference between rays with $\zeta = 0$ and $\zeta = 90$; this value is given by $2e$. Parameter a has the same effect on all ray angles and therefore does not cause any change in velocity with changing ray angle. Parameter f describes how rays with intermediate ray angles are different to those with equatorial or polar angles, as such it does not provide a contribution to the differences between polar and equatorial paths. Here, variation in a or f is not individually examined; this may be considered in future work. In particular, the strength of coefficient f relative to e will determine the angle of the slowest velocity anomaly, which may prove to be important when comparing results from seismology with data from mineral physics (Lythgoe et al., 2014).

The Voigt isotropic velocity, which is the velocity averaged over all spherical angles, can then be written as:

$$\left(\frac{\delta v}{v}\right)_{voigt} = a - \frac{e}{3} - \frac{f}{15} \tag{2}$$

using the same dimensionless parameters (this can be obtained from rewriting equation A3 of Creager (1999)).

Differential travel time predictions for the ak135 model (resampled every 25 km in the inner core Kennett et al. (1995)) were calculated for each seismogram. Differential travel time residuals are then the difference between observed and predicted differential travel times; in this work are always relative to resampled ak135 and corrected for ellipticity. In Section 3.1 the data are analyzed as a function of ζ, position and turning depth in the inner core.

2.2. Inversion method

Travel time perturbations in the inner core caused by velocity anomalies are calculated by dividing each ray in the inner core up into 'legs' which each cover 25 km in depth. Each leg is assigned to the correct region of the inner core using the geometrical midpoint along the leg, and the relevant values of the coefficients a, e and f of Eq. (1) are then used to determine the anisotropy that each leg of the raypath experiences. Dividing the ray path up into up to 30 legs in the inner core allows a much better resolution of the true effect of inner core boundaries than previous studies which simply used the turning point of a ray to assign it to a hemisphere of the inner core. Using a layer thickness of 25 km, the longest leg in the inner core is 227 km and the median leg length is 54 km. When the data are inverted, values of the parameters a, e and f are sought for all of the required sub-regions of the study area using an iterated least-squares inversion; with 2471 datapoints and fewer than 25 variables sought in the inversion, no damping is used. The leg-binning method described above is used to find contributions to the derivatives of coefficients a, e and f in the inversion. Ray-paths used in each case are those in the isotropic starting model. Data variance reduction is used to indicate how much an anisotropy model improves the fit between the predictions and observations. Data variance is given by the sum of the squared difference between the predicted and observed differential travel times, divided by the number of data points. When no anisotropy model is used, the data variance is 0.13 s^2; all variance reductions caused by the introduction of inner core anisotropy models are relative to this value.

3. Results

3.1. Differential travel time residuals

The dataset created consists of 2471 differential travel times. When the differential travel time residuals are plotted as a function of ζ, anisotropy in the inner core is apparent – paths with smaller ζ generally have more positive differential travel time residuals than paths with larger ζ. The amount of anisotropy present is quantified in Sections 3.2 and 3.3.

The geographical distributions of the PKPdf turning points as a function of depth and ray paths in the inner core is shown in Fig. 5. The ray angle used to define polar paths varies between different studies. Polar data, defined here as paths with $\zeta < 40$ (Fig. 5a), are sparser than the equatorial data (Fig. 5b). There are 223 polar data, 35 of which have $\zeta < 30$ and one of which has $\zeta < 24$. Differential travel time residuals for the polar data are −0.6–3.3 s; for the equatorial data they range from −1.3 s to 1.2 s. Both the highest and lowest polar differential travel time residuals are close to the western-most end of the cross-section. While all of the rays turn between 30°W and 60°E, it can be seen that they sample the inner core beyond both of these boundaries (Fig. 5c).

A strong trend in differential travel time as a function of PKPdf turning depth in the inner core would indicate that the underlying

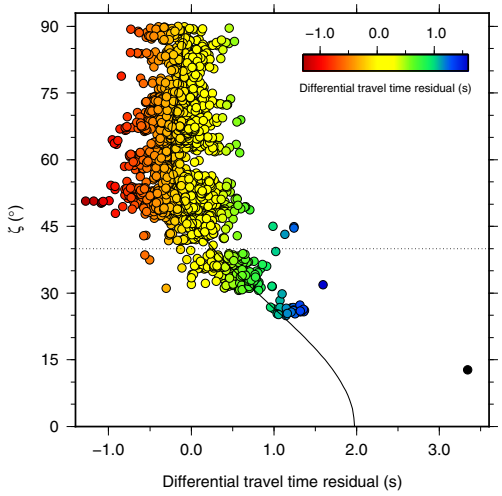

Fig. 4. Differential travel time residuals, relative to ak135 predictions and corrected for ellipticity, plotted as a function of ζ. The dotted line at $\zeta = 40$ indicates the division between polar and equatorial data. Positive differential travel time residuals correspond to an inner core with a higher than predicted velocity. The solid line shows the predicted differential travel time residuals for the best fitting uniform anisotropy model, calculated for an epicentral distance of 151.29° and a source depth of 100 km (see Section 3.2 for more information).

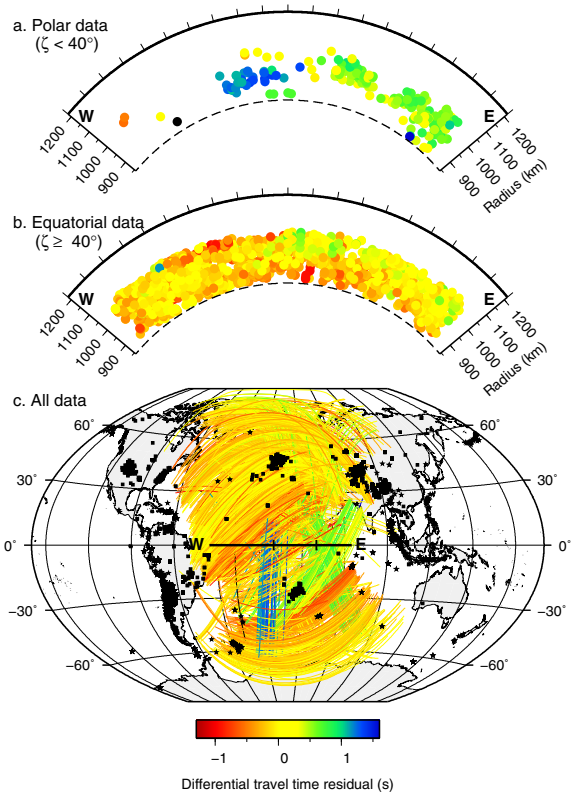

Fig. 5. Differential travel time residuals in cross-section and map view. Turning points of PKPdf in the inner core are projected onto a cross-section from 35°W, 0°N to 65°E, 0°N for (a) polar and (b) equatorial paths. Entire inner core paths of PKPdf are shown as colored lines in (c), with stations indicated by squares and earthquakes by stars. Tick marks are shown every five degrees from 35°W to from 65°E in the cross sections (a) and (b), tick marks shown on the cross section line correspond to longitudes 10°E and 40°E. A map view of the polar data alone is shown as Supplementary Fig. S4. Note that the color scale used is saturated at the higher end. (For interpretation of the references to color in this figure legend, the reader is referred to the web version of this article.)

1D velocity model used was inappropriate; either in terms of the velocity profile of the inner core, affecting calculations of PKPdf travel time, or in the lowermost outer core where PKPbc turns. Here, velocity model ak135 is used to represent 1D Earth structure, and the differential travel time residuals relative to this model as a function of turning depth are shown in Fig. 6. Scatter in differential travel time residuals is present at all turning depths, with more positive differential travel time residuals often corresponding to paths with lower ζ. No large scale linear trend is evident in this data, suggesting that the 1D reference model used is reasonable. To confirm this, a linear fit to the data shown in Fig. 6 was calculated. The best fit line has a differential travel time residual of 0.0 s for a turning depth of 150 km, meaning that the observed and predicted differential travel times are equal, and has a gradient of only -0.08 s/100 km. A simple fit of differential travel time residual to turning depth cannot, however, take into account the range of ray angles present at different depths, and therefore should not be used to investigate isotropic velocity. Inner core Voigt velocity anomalies are investigated in Sections 3.2 and 3.3 below.

This dataset can be compared to two earlier published studies using PKPbc–PKPdf data, both of which were considering the evidence for inner core differential rotation. Souriau and Poupinet (2003) used data which sampled the inner core under western and central Africa. Polar paths had differential travel time residuals of over four seconds for the smallest ray angles, while paths with $\zeta > 40$ all had differential travel time residuals within ± 1 s of ak135 predictions, a slightly smaller range than that found here. That study used 81 points, and sampled a much smaller geographical region, so that this slightly tighter clustering is not surprising. The anisotropy model of Souriau and Poupinet (2003) is compared to the models retrieved in this study in Section 4.1. PKPbc–PKPdf differential travel time measurements corresponding to nuclear explosions in Novaya Zemlya, detected at stations SNA (9 datapoints) and NVL (21 datapoints), are published in Li and Richards (2003). The ray angles of these paths are 9.0° and 6.9° for the two stations and show travel time anomalies of 3.0% and 3.1% relative to iasp91 (Kennett and Engdahl, 1991). These travel time anomalies are slightly larger than the 2.2% fractional travel time anomaly experienced by the most polar of the paths in this dataset, but given the lower ζ and different reference model for these data, they are broadly consistent.

3.2. Inversion of all data

As a first step, the whole dataset is inverted for uniform anisotropy across the study region in one or two layers (Fig. 7). When two layers are used, they are divided 250 km below the ICB. The division at 250 km both reflects a depth where several authors have suggested a change in inner core properties (Song and Xu, 2002; Tanaka, 2012; Miller et al., 2013) and also means that roughly half of the data turns in each layer.

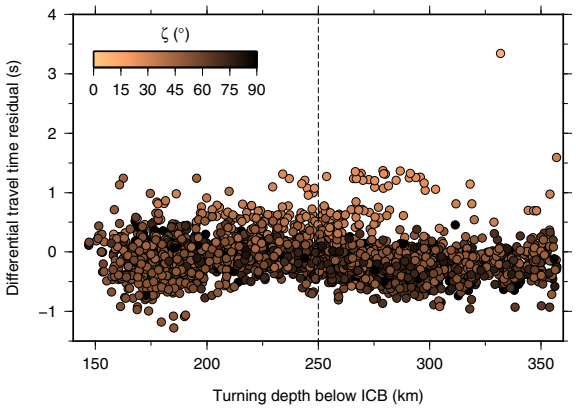

Fig. 6. Differential travel time residuals plotted as a function of turning depth below the ICB. The dotted line indicate the layers used when the data are inverted for inner core anisotropy with two layers.

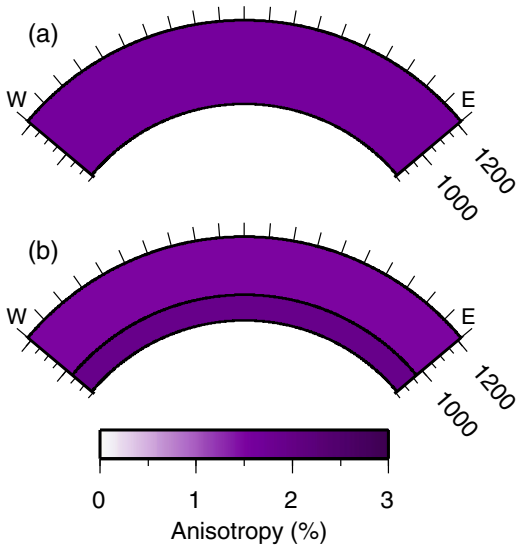

Fig. 7. Inner core anisotropy when considering (a) no variation as a function of depth, (b) two layers. The uppermost arcs in each image correspond to the ICB, the lower arcs divide the inner core into the relevant layers.The letters W and E correspond to the ends of the cross-section shown in Fig. 5 and the radial axes correspond to radius in the Earth.

Inverting the whole dataset together reveals 1.6% anisotropy under African and the surrounding regions. When two-layered structure is permitted, the anisotropy present is higher at greater depths (1.9%), and slightly lower in shallower regions (1.5%). A test inversion of hemispherical data (see Section 3.4.1 below) suggests that this kind of layered structure may be retrieved in an undamped inversion of hemispherical, un-layered data, so that the two-layer result cannot be treated as robust. If a laterally varying structure is present, both layers and lateral variation must be inverted for in order to prevent the misattribution of lateral structure to radial variation.

Depth dependence of anisotropy has been observed by a number of previous studies, here it is shown that on average the study region has increasing anisotropy with increasing depth below the ICB. When anisotropy is permitted in the inner core, variance is reduced by 52%, and 54% for the one and two layer models respectively. Permitting anisotropy in the inner core clearly represents the data better than using ak135, however the improvement in variance is small when a second layer is permitted, showing that radial variation in anisotropy is not a prominent feature when lateral variation of anisotropy is ignored.

Differential travel time predictions made using the best fitting one layer anisotropy model are shown in Fig. 4. These predictions have been made using a representative source depth of 100 km and the median epicentral distance of the data used (151.29°). The line corresponds to a PKPdf wave which spends 131 s in the inner core and turns 250 km below the ICB. The line appears to fit the overall trend of the data well; it underestimates the data with $\zeta < 30$, which is to be expected, because 80% of these data correspond to paths with larger epicentral distances and one would therefore expect them to accrue larger differential travel times residuals than for the path shown. The very polar path with $\zeta = 12.77$ is significantly underestimated by this model; the effect of this datapoint is discussed in more detail in Section 3.4.2 and in Section 2 of the Supplementary materials.

The Voigt isotropic velocities for the models are close to zero, with slightly higher velocities in the shallower layers. For the one layer model $(\delta v/v)_{voigt} = 0.1\%$. When two layers are permitted, the upper layer has a Voigt anomaly of 0.1% while the lower layer anomaly is 0.0%. As suggested by analyzing differential travel times as a function of turning depth (Fig. 6), the results of the inversion make it evident that: (i) ak135 is a suiTable 1D reference model and (ii) when lateral variation is not considered data are better fitted when the upper parts of the inner core have slightly higher velocity perturbation than the region immediately beneath them.

3.3. Inversion for longitudinally varying structure

After ascertaining that anisotropy is present in the study region, models where anisotropy is permitted to vary as a function of longitude are sought. The parameterization used is one of constant anisotropy in blocks, with the blocks divided by lines of longitude at either 10°E and 40°E, or at 10°E, 30°E and 50°E. While all of the data with $\zeta < 30$ turn west of 20°E, there are more than 30 paths with $\zeta < 40$ and 10 paths with $\zeta < 35$ which turn in each of the longitudinal blocks used; the range of turning depths present in each block varies (Fig. 5a and Supplementary Tables ST3 and ST4). The west-most block is larger than the other two blocks but is not divided further as this would result in a very low number of polar legs present in the newly-created blocks (see Fig. 5).

In the one layer inversions, (Fig. 8a and c) anisotropy is stronger in the west and center than in the east-most block. This matches the globally observed pattern of hemispherical variation (Table 1), but the amplitudes are more similar than in several global studies – 1.7–1.8% in the west and 0.5–0.8% in the east. This shows that the western hemisphere under Africa is less anisotropic than under Central America. In the two layer inversions, it is evident that the anisotropy in the eastern end of the study area increases with depth, thus there is depth dependent anisotropy in the study region. In both the three and four block models the anisotropy is higher in the lower layer than in the upper layer at all longitudes. Robustness tests (Section 3.4) suggest that anisotropy is better constrained in the upper layers where there is more data. The variance reduction for the three block, two layer, model (Fig. 8b), 59%, is the same as for the four block, two layer model (Fig. 8d), so that slightly increasing the permitted model complexity cannot fit the data better. Statistical tests (see Supplementary materials) show that the four block one and two layer models do not improve the fit, either at all, or sufficiently to justify their use over the three block one layer and three block two layer models respectively. The anisotropy, Voigt velocity anomaly and variance reduction ranges for all of the models are given in Table 2. The African hemisphere boundary location varies as a function of depth in the study region, and cannot be represented by one line of longitude. The region of highest anisotropy is in the lower center of the model but the anisotropy retrieved there is lower than under Central America. Overall, the pattern of anisotropy seen in the inner core shows weak anisotropy in the east of the study region, especially in the upper part of the inner core, and intermediate strength anisotropy in the 'western' parts of the study region with some variability present.

In the one layer inversions (Fig. 8a and c), Voigt anomalies are small and 0.1% to 1 decimal place in all cases, with a range of 0.1%; no hemispherical Voigt variation is apparent. In the two layer inversions (Fig. 9b and d), negative Voigt velocities mostly correspond to regions with stronger anisotropy. Anomalous recovery of Voigt velocities in the presence of strong anisotropy was evident in the synthetic tests, so that the signals cannot be considered robust. Despite this, no strong isotropic hemispherical pattern is apparent in these two layered models either; the Voigt isotropic anomaly in the parts of the model which are identified as being in the eastern hemisphere (using the anisotropic model) are not different to the anomalies in the parts of the model identified as being in the western hemisphere (Table 2). In the one and two layer inversions, it is apparent that Voigt isotropic and anisotropic structures cannot be considered to have the same geographical

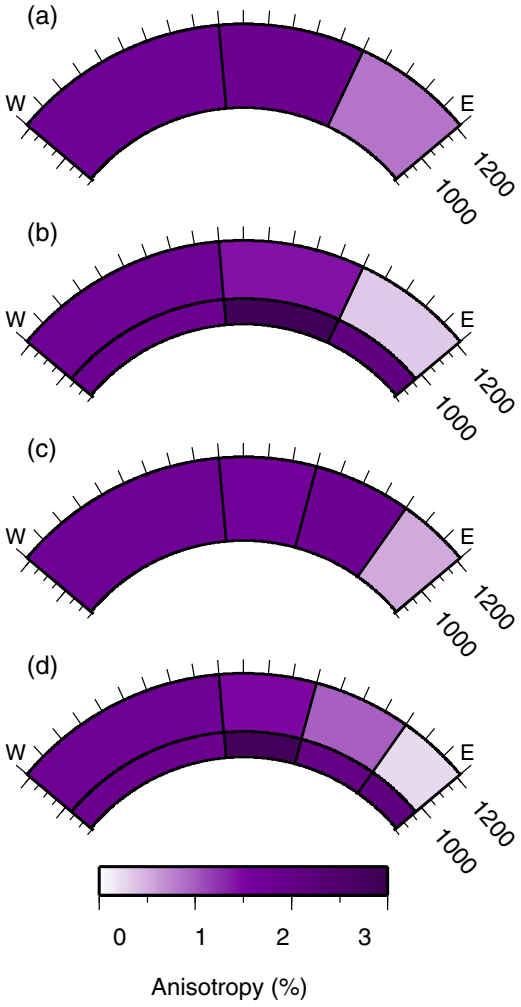

Fig. 8. Inner core anisotropy when considering three lateral blocks and (a) one or (b) two layers, and four lateral blocks and (c) one or (d) two layers. The uppermost arcs in each image correspond to the ICB, the lower arcs divide the inner core into the relevant layers.The letters W and E correspond to the ends of the cross-section shown in Fig. 5.

Table 1
Anisotropy either side of the African hemisphere boundary. Results from Creager (1999), Leykam et al. (2010) and Irving and Deuss (2011) are those obtained using PKPdf–PKPbc data. The value for Lythgoe et al. (2014) corresponds to the uppermost 467.5 km of the inner core, that of Sun and Song (2008) is an estimate of the anisotropy in the two hemispheres at 300 km below the ICB (from their Fig. 17). In the one block model, the easternmost block is considered to be in the eastern hemisphere, however for the two layer model, only the upper easternmost block is representative of the eastern hemisphere and the lower easternmost block is considered to be part of the western hemisphere.

Study	East. H. Ani (%)	West. H. Ani (%)
Creager (1999)	0.5	4.0
Sun and Song (2008)	0.8	2.9
Leykam et al. (2010)	0.4	–
Irving and Deuss (2011)	0.5	4.8
Lythgoe et al. (2014)	1.4	3.5
This study (3 block model)		
One layer model	0.8	1.7–1.8
Two layer model	0.4	1.4–2.9

Table 2
Anisotropy, Voigt isotropic velocity anomaly and variance reduction for each model. Eastern and western hemisphere are defined as in Table 1 for the two layered models. The four block models, indicated by *, do not provide a significant (or any) improvement in fit over the three block models despite their increased level of complexity.

Parameterization		East. H. Ani. (%)	West. H. Ani. (%)	East. H. Iso. (%)	West. H. Iso. (%)	Variance Red. (%)
One block	One layer	1.6		0.1		52
	Two layers	1.5–1.9		0.0–0.1		54
Three blocks	One layer	0.8	1.7–1.8	0.1	0.1	54
	Two layers	0.4	1.4–2.9	0.2	−0.4–0.2	59
Four blocks	One layer*	0.5	1.7–1.8	0.1	0.1	54
	Two layers*	0.2	1.0–2.8	0.2	−0.4–0.2	59

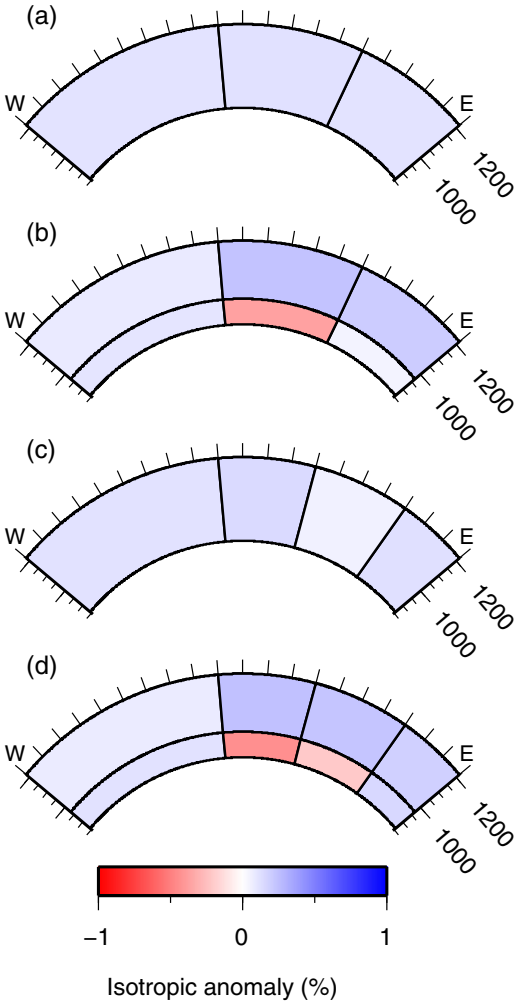

Fig. 9. Inner core Voigt isotropic velocity when considering three lateral blocks and (a) one or (b) two layers, and four lateral blocks and (c) one or (d) two layers. The uppermost arcs in each image correspond to the ICB, the lower arcs divide the inner core into the relevant layers. The letters W and E correspond to the ends of the cross-section shown in Fig. 5.

distribution. Several previous studies have found that Voigt velocities in the eastern and western hemisphere are the same (Creager, 2000; Garcia and Souriau, 2000, 2001; Sun and Song, 2008); the one layer results support this finding on a regional scale. The absence of variation in Voigt velocities in the one layer inversions suggests strongly that the anisotropy observed is due to differing alignments of anisotropic grains and not to intrinsically different materials (Garcia, 2002b).

3.4. Robustness of results

The data coverage in the inner core is not ideal – the polar paths, which are more strongly affected by cylindrical inner core anisotropy, are not uniformly distributed (Fig. 5a and Supplementary Fig. SF4). This is primarily due to the combination of the uneven distribution of earthquakes with suitable size and focal mechanisms to provide clear PKPdf and PKPbc signals and the uneven distribution of broadband seismic stations (respectively shown by stars and squares in Fig. 5c and Supplementary Fig. SF4). The imperfect distribution of paths means that the sampling of the inner core is uneven. The requirement that data from the same event cannot have both the same epicentral distance and ζ (Section 2.1) prevents raypaths from one event completely overlapping. Here two tests are carried out to investigate (i) how well the data coverage can recover an input model with different parameterization and (ii) how the inversion results change as a result of removing the most extreme datapoint.

3.4.1. Inversion of synthetic data

To investigate whether the dataset used would be able to retrieve hemispherical anisotropy in the inner core, synthetic data was inverted for (i) layered anisotropy with no lateral variation and (ii) laterally varying anisotropy. The synthetic data was created using the PKPbc–PKPdf anisotropy model of Irving and Deuss (2011), with 4.8% anisotropy in the western hemisphere and 0.54% in the eastern hemisphere (Fig. 10a). The hemisphere boundary was placed at 40°E, the modal boundary locations of previously reported results shown in Fig. 1. When input anisotropy has the same boundaries as used in the inversion, the input model is retrieved.

When hemispherical anisotropy was present in the study region and an inversion for uniform lateral structure and two radial layers was carried out, the inversion resulted in an anisotropy model with lower anisotropy in the upper layer, and higher anisotropy in the lower layer (Fig. 10b). This mis-attribution of the lateral input structure into radial output structure means that a two-layer uniform anisotropy model retrieved should not be considered robust, as discussed in Section 3.2. When the boxes used in this inversion do not mirror the input hemisphere boundary, as expected the anisotropy retrieved shows smearing across the true boundary (Fig. 10c). The anisotropy in the easternmost panels is slightly underestimated (retrieved anisotropy is 0.0% and −0.1%) and that anisotropy in the lower center-left block is slightly higher than the input anisotropy (5.1% instead of 4.8%). Nonetheless, the overall pattern of anisotropy input is retrieved, providing confidence in the results of the inversion. In the same inversions, input isotropic Voigt velocities (Fig. 11a) are mostly well recovered (Fig. 11b), but the lower center blocks see anomalous signals (Fig. 11c), so Voigt velocities should not be regarded as robust there. The same problem is not evident in the un-layered inversion, so these Voigt velocities are more likely to be robust.

3.4.2. Removing the most polar path

Only one datapoint has $\zeta < 24$. This corresponds to an earthquake in central Iceland in October 2014 which was recorded at station SPOLE (89.93°S, 144.44°E; $\zeta = 12.77$). Though this is only

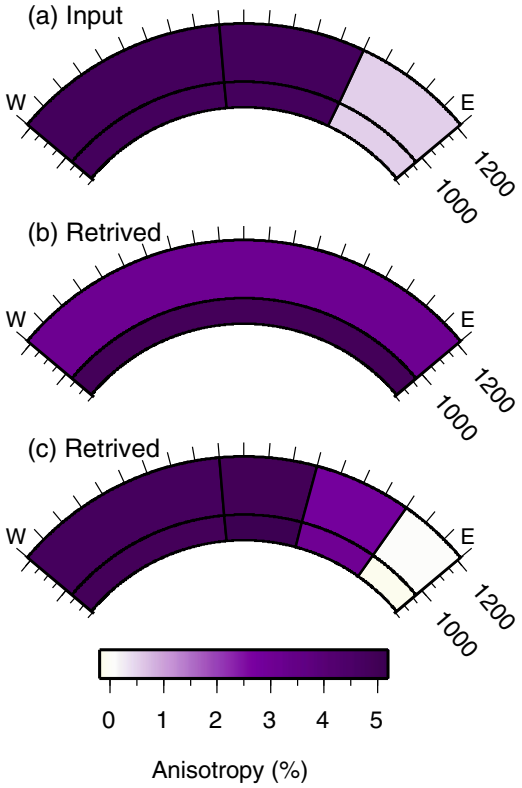

Fig. 10. Inner core anisotropy (a) input to create synthetic data, (b) retrieved in a two layer inversion with no lateral variation permitted and (c) retrieved in a two layer inversion with four lateral blocks used. The uppermost arcs in each subfigure correspond to the ICB, the lower arcs divide the inner core into the relevant layers. The letters W and E correspond to the ends of the cross-section shown in Fig. 5. Note that the color scheme used here is not the same as that in Figs. 7 or 8.

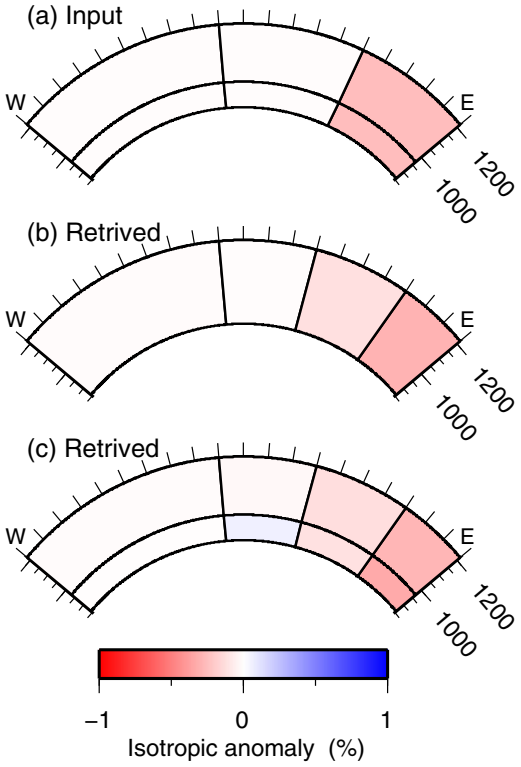

Fig. 11. Inner core Voigt isotropic anomalies (a) input to create synthetic data, and retrieved in a (b) one layer and (c) two layer inversion with four lateral blocks used. The uppermost arcs in each subfigure correspond to the ICB, the lower arcs divide the inner core into the relevant layers.The letters W and E correspond to the ends of the cross-section shown in Fig. 5.

one datapoint in 2471 it is prudent to examine the effect that this extreme datapoint has on the results of this study. No other events produced usable records at SPOLE; one similar earthquake produced waveforms which could not be satisfactorily picked. Inversions were therefore carried out without the SPOLE datum. This datum is discussed further in the Supplementary materials; the seismogram corresponding to this event, as well as the earthquake moment tensor are shown in Supplementary Figs. S3 and S2 respectively. When the whole dataset is inverted, inner core anisotropy remains at 1.6% (the decrease in anisotropy is −0.03%). When lateral variation in the inner core is permitted, removing this seismogram has limited effects on the anisotropy retrieved, with changes less than 0.1%. Changes are larger in the models with both depth and lateral variation of anisotropy; in both the six and eight block parameterizations the lower model block in which the SPOLE ray turns has 0.6% less anisotropy when that seismogram is not included; other changes are of the order of 0.1% or less. The Voigt isotropic anomalies change by 0.1% or less in all blocks when this data point is removed. From this test it can be concluded that anisotropy in the lower layer may be less robustly resolved than in the upper layer.

4. Discussion & analysis

4.1. Comparison with previous studies

Several previous studies concentrate on the inner core around the African hemisphere boundary; two studies estimate the anisotropy under the whole of Africa. Eighty-six PKPbc–PKPdf differential travel times corresponding to paths turning under equatorial Africa were used by Souriau and Poupinet (2003), to find the anisotropy in that region. The authors assumed that the uppermost 100 km of the inner core were isotropic, and found that the anisotropy below this layer was 3.2%. At an epicentral distance of 150° for an earthquake at a depth of 100 km, this anisotropy model would predict a travel time anomaly of 1.0 s for a path with $\zeta = 30°$, which is comparable to measurements in the dataset used here. Using a similar assumption of a 100 km thick isotropic layer, Ovtchinnikov et al. (2012) found that below 100 km the anisotropy was 4.33%; this model would produce a travel time anomaly greater than the anomalies present in this dataset for similar ray angles. Both of these studies report higher anisotropy than that detected here, but that is because they required the upper 100 km to be isotropic, as suggested by Song and Richards (1996), following Shearer (1994). However, Yu and Wen (2007) found that under some parts of Africa the isotropic layer is thin or absent, and the isotropic western hemisphere layer of Waszek and Deuss (2011), which includes much of the region under Africa has an isotropic layer thickness of 57.5 km, close to half the size of that assumed by Souriau and Poupinet (2003) and Ovtchinnikov et al. (2012). The PKPdf waves travel at a steep angle through this thin layer; a ray which turns 250 km below the ICB spends only 15.3 s of its 131.5 s transit of the inner core in the uppermost 50 km. An uppermost isotropic layer would therefore have only a small effect on the travel time of PKPdf in the inner core, and such a layer is therefore not explicitly modeled in this study, though it is a topic for future investigation. The absence of such a layer may cause a slight underestimate in the anisotropy in the remainder of the top layer of the models produced here.

One of the most detailed studies of the inner core under Africa is that of Yu and Wen (2007), which uses 308 records of polar PKPdf

and PKiKP waveforms which turn in the uppermost 80 km of the inner core under Africa. The data, generated by earthquakes in the South Sandwich Islands, are split into six bins; each polar PKPdf path is entirely within one bin. The study estimates both the thickness of any isotropic layer and the anisotropy present below any isotropic region. An isotropic layer is found in the western bins, but is not present in the two easternmost bins beyond roughly 30°E. Anisotropy below a 40–50 km thick isotopic layer varies from 1.6% to 2.2%. The anisotropy is generally higher towards the eastern part of the region sampled, but there is not a consistent trend in anisotropy strength as a function of longitude. This anisotropy is of a similar strength to that found here, and suggests that there is nor a significant amount of depth dependent variation in inner core anisotropy from 80 km (the deepest part of the inner core sampled in that study) to the deeper regions probed in this study. This is in contrast to the inner core under Central America, where an increase in anisotropy 100–250 km below the ICB is inferred from an increase in velocity for polar paths (Song and Helmberger, 1998; Blom et al., 2015).

Miller et al. (2013) sampled the inner core using waveforms from 24 Indonesian archipelago events recorded in the southeastern Caribbean, turning up to roughly 300 km below the ICB. Their model has a +0.5% velocity anomaly in the eastern hemisphere (relative to PREM Dziewonski and Anderson, 1981) whilst the western hemisphere has a -0.5% anomaly. These travel time anomalies persist down to 150 km and 250 km below the ICB for the eastern and western hemispheres respectively. This study also reveals a 'step-like' change in inner core Properties 5° from that imaged by Miller et al. (2013), though the parameterization used here is relatively coarse.

To summarize, this study samples the inner core under Africa with many more waveforms than has previously been used. Previous studies are mostly in agreement with the new results; travel-time anomalies are similar to predictions by Souriau and Poupinet (2003) and anisotropy observed is similar to that found by Yu and Wen (2007), but lower than that reported by Ovtchinnikov et al. (2012); changes in inner core anisotropy are seen in a similar place to the equatorial results of Miller et al. (2013) but the depth extent of the variations is different.

4.2. Interpretation

The inner core under Africa is anisotropic, but on average it is much less anisotropic than the western hemisphere is often found to be (Table 1). While some studies raise concerns about the dominance of South Sandwich Islands – Alaska paths on the estimation of western hemisphere anisotropy (e.g. Romanowicz et al., 2003; Tkalčić, 2010), the observation of large scale odd degree structure in normal mode splitting functions provide evidence of quasi-hemispherical structure in the inner core which is difficult to refute. It therefore appears that the inner core under most of Africa exhibits anisotropy which is smaller in amplitude than in the western hemisphere under central America, but stronger than in the eastern hemisphere. The anisotropy is 1.4–2.9% throughout much of the study region, but is lower in the east-most upper block of the inversion when a layered inversion is carried out. Anisotropy is therefore laterally and radially varying in the upper 360 km of the inner core.

To create seismic anisotropy, lattice preferred orientation of inner core crystals is likely to be required. Shape preferred orientation of ellipsoidal fluid inclusions in the inner core has been suggested (Singh et al., 2000), but it is difficult to see how such fluid inclusions would be maintained at substantial depth in the inner core, where anisotropy is known to persist (see, for example, Sun and Song (2008) and Lythgoe et al. (2014)) and so this anisotropy mechanism is not considered further. Anisotropy mechanisms which could align the inner core crystals primarily use either magnetic or thermal deviations from spherical symmetry in the core either to align crystals as they grow, or to align already existing crystals [see Sumita (2007) and Alboussière and Deguen (2012), for reviews of these mechanisms].

A good understanding of the thermal evolution of the core will allow us to understand the age of crystals in our study region. For more than a decade an inner core age of about 1000 Myrs (Labrosse et al., 2001) was considered to be a reasonable estimate, though significant uncertainty was attached to this number. Experimental and theoretical estimates of the conductivity of iron under core conditions have since increased by a factor of two or more (de Koker et al., 2012; Pozzo et al., 2012; Gomi et al., 2013). The altered estimates of the conductivity of iron have also led to the conclusion that previous inner core ages estimates are likely to be too large, though the high conductivity estimates have lead to concerns about how to power the early dynamo (for a summary, see Olson (2013)), and two recent computational and paleomagnetic studies have cast some doubt on these very high values of conductivity (Zhang et al., 2015) and low inner core age (Biggin et al., 2015) respectively. The new conductivity measurements, combined with a model of the core's thermal evolution lead to the proposal that the inner core must be younger than 700 Myr (Labrosse, 2015). Using this age and Eq. (41) of Labrosse (2015), the top 360 km of the inner core grew in the past ~410 Myr or less, and the uppermost 250 km in the past ~310 Myr or more recently. Even lower inner core ages (as summarized in Davies et al. (2015)) will clearly reduce the age of the study region.

Paleomagnetic studies indicate the presence of a dynamo for most of Earth's history (Tarduno et al., 2015), with a dipolar signature present since before the inner core nucleated (Smirnov and Tarduno, 2004). Anisotropy mechanisms invoking the magnetic field (Karato, 1993; Karato, 1999; Buffett and Wenk, 2001) would be see the dominant dipole and it is difficult to see how they could create laterally varying anisotropy in the inner core under such conditions. Magnetic texturing of the inner core is therefore unlikely to cause the observed variability in anisotropy.

The remaining plausible anisotropy mechanisms therefore depend on variations in the thermal environment of the core causing variations in anisotropy either via a post growth deformation mechanism or during inner core growth. Thermal mechanisms can also be divided (following Lasbleis and Deguen (2015)) into those caused by influences external to the inner core – especially inhomogeneous heat fluxes imposed upon the core – and those intrinsic to the inner core – for example inner core convection.

Gross convection in the inner core has been invoked to explain anisotropy (e.g. in Jeanloz and Wenk (1988) and Romanowicz et al. (1996)) whereby the convective processing of the inner core results in crystal alignment. An inner core with a supercritical Rayleigh number (Jeanloz and Wenk, 1988) and a suitable deformation behavior (Wenk et al., 1988) could create a cylindrical anisotropic texture. For convection to be possible, inner core viscosity would have to be sufficiently low for this mode of heat transport to occur, the inner core would need to be superadiabatic for thermal convection to occur, and any compositional stratification which may be present must be overcome. Buffett (2009) found that convection was possible early in the inner core's history, in a mode which could align inner core crystals, but would be suppressed as the inner core grew; this cessation of convection as the inner core grew was also possible in the modeling of Deguen and Cardin (2011), who emphasized that the convection regime in the inner core depends on parameters which are poorly known, including inner core viscosity. In a similar vein, Cottaar and Buffett (2012) showed that thermochemical convection is possible for some combinations of geophysical parameters (specifically low conductivity of iron and high CMB heat flux). Using new values of iron's conductivity,

Lasbleis and Deguen (2015) show that the inner core may be convecting or stably stratified, and that one of several different deformation and texturing mechanisms could be at dominant in the inner core. Gross convection could therefore exist in the inner core, but it is not apparent how convection could vary laterally to cause the observed variation in inner core anisotropy.

A relatively viscid inner core could instead favor inner core translation (Alboussiere et al., 2010; Monnereau et al., 2010) as a convective mechanism, where individual crystals are transported from the inner core under the Americas to under Asia, where they melt and become part of the fluid outer core. Initial studies of inner core translation were unable to explain inner core anisotropy, though Mizzon and Monnereau (2013) subsequently suggested that flows in the growing uppermost western hemisphere could be responsible for texture which was removed by annealing as translation proceeded. However, if a texture has been created during solidification, whether it is erased or can persist is not certain (as shown in analog material studies by Bergman et al. (2010) and Al-Khatatbeh et al. (2013)). Material which has been partially melted from above may also produce a different density signature, and therefore isotropic velocity, to material which has directionally solidified (Yu et al., 2015). As the one layer Voigt isotopic velocity model found here shown no lateral variation if some of the study are has undergone melting this effect, if present, must produce very small changes in inner core properties. Further studies of the consequences of directional solidification and melting, such as these experimental ones, will no doubt cast further light on the processes which may be at work in the inner core.

There have recently been a number of studies which consider the impact of inhomogeneous heat flow at the core-mantle boundary (CMB), caused by the heterogeneous lower mantle, on the heat flux at the ICB. An early laboratory model (Sumita and Olson, 1999) found that a high heat flux at the CMB would produce rapid solidification at the opposite side of the inner core. This experiment used a very high contrast between the highest and lowest heat fluxes, with the peak flux 95 times the mean. It is not clear how physically realistic such a heat flux range is. The benefit of laboratory modeling is that small scale features can be captured, unlike in computational studies where the scale is limited by the number of grid points used.

More recent computational studies using more sophisticated models of CMB heat flux heterogeneity (Aubert et al., 2008; Gubbins et al., 2011; Sreenivasan and Gubbins, 2011; Driscoll, 2015) have found that the relationship between the CMB and ICB heat fluxes is more complex, with thermal winds in the outer core communicating imperfectly between the two interfaces. All four studies use mantle tomography shear wave velocity models to simulate variation in heat flux at the CMB; these models represent the long wavelength velocity structure of the lower mantle, but do not distinguish between thermal and chemical causes of mantle velocity perturbations, and do not capture small scale but strong heterogeneities such as ultra low velocity zones (ULVZs). Two of these studies find that the heat flux variation at the ICB may be sufficiently large that the parts of the ICB are the location of inner core melting, and not growth: Gubbins et al. (2011) and Sreenivasan and Gubbins (2011) find that, depending on the strength of lateral CMB heat flux variation, the ICB may be either growing or melting under Africa. Aubert et al. (2008) predicts similar heat fluxes, and therefore inner core growth rates under both Africa and Central America. The recent work of Driscoll (2015) reports complex variations in ICB heat flux; the heat flux under the eastern North and Central Atlantic and Western Africa is lower than that under the rest of Africa and the western Indian Ocean. Driscoll (2015) reports that the differences between that work and Aubert et al. (2008) may be due to different ways of treating compositional variation. CMB heat flux lateral variations imposed in calculations were much smaller than in the laboratory experiments of Sumita and Olson (1999), ranging from a peak-to-peak amplitude difference of 15% of the mean heat flow (the lower value used by Gubbins et al. (2011) and Sreenivasan and Gubbins (2011)) to spherical harmonic contributions of more that 140% of the average flux (Driscoll (2015)). Driscoll (2015) finds that smaller scale CMB structures, represented by higher order spherical harmonics (in this case order 5–8 spherical harmonics), can have an effect on the heat flux at the ICB. As the laboratory modeling (Sumita and Olson, 1999) also found the presence of small scale feature, future, higher resolution experiments and computations of heat flux at the ICB are desirable to better understand dynamical processes occurring at and below the ICB. The laboratory and computational studies provide evidence that anticipated heat flux variations at the CMB will cause changes in the heat flux at the ICB, though the relationship between CMB and ICB flux is not a 1:1 correspondence.

If the variation in inner core anisotropy is indeed caused by heterogeneous CMB heat flux, then either solidification texturing (Bergman, 1997) may cause the anisotropy (as favored by Aubert et al. (2008)), or alternatively post-crystallization deformation (Yoshida et al., 1996) may be the anisotropy mechanism. The former mechanism would require that the growth of inner core crystals is faster in the upper east of the study region; it would require that the texture imprinted at solidification is not destroyed by any solid-state flow in the inner core (Bergman, 2003). The latter mechanism would instead indicate that the inner core is growing less quickly under this region, and there is therefore less deformation of the region, resulting in a lower degree of alignment of crystals which were initially isotropically oriented. The main limitation of this theory is that it may act too slowly to create the texture observed in the inner core (Yoshida et al., 1998).

A good test of some of these anisotropy-forming mechanisms would be to investigate the latitudinal variation of inner core anisotropy, as well as the longitudinal changes. Changes in anisotropy most strongly affect polar paths, which are not present near the poles due to geometrical restrictions. With an ideal distribution of data across the inner core it might be possible to probe latitudinal anisotropy variations. However, due to the locations of suitable events and seismic stations, the polar paths present in the data (Supplementary Fig. S4), especially those with $\zeta < 35$, have similar latitudinal profiles are therefore poorly suited to investigating latitudinal variations in anisotropy. Such variations in anisotropy should be the targets of future seismological investigations of inner core structure.

If the assumption is made that the low anisotropy region under the eastern Indian Ocean is caused by a heat flux anomaly at the CMB, then two interpretations are possible. The first is that the degree of solidification texturing at the ICB in this region must have been different while the top 250 km of the inner core were formed. The second is that the post-solidification deformation taking place must have been stronger in the inner core under Africa than in the inner core under the eastern Indian Ocean over a period of time long enough to affect the top 250 km. As post-solidification deformation is a slow process, the thermal conditions must have been different for an extended period of time, with an upper limit of the age of the uppermost 250 km. Both interpretations therefore favor a heterogeneous heat flux at the CMB for a period of time reaching up to 310 Myrs, as suggested by some reconstructions of mantle behavior (Torsvik et al., 2010).

5. Conclusions

The inner core under Africa and surrounding regions has been sampled with an unprecedentedly large dataset comprising almost 2500 differential travel time residuals. Anisotropy present is

weaker than in the inner core under Central America. Most of the study region shows intermediate levels of anisotropy, varying from 1.4% to 2.9%, however the upper inner core under the western Indian Ocean shows weaker anisotropy, leading to the conclusion that anisotropy varies both laterally and radially under the study region. If one line of longitude is needed to represent the hemisphere boundary, then 40°E is a better boundary location than 10°E, however the depth variations in the inner core mean the boundary therefore cannot be truly represented by one line of longitude. Voigt isotropic velocities for a one-layer laterally varying model show no evidence of hemispherical variation indicating that the hemispherical signal is present only in inner core anisotropy, and is therefore due to a difference in crystal alignment and not due to the presence of different material. The most likely cause of the observed lateral variation of anisotropy in the inner core is a heterogeneous CMB heat flux which has remained stationary with respect to the inner core for hundreds of millions of years.

Acknowledgments

Data have been collected from networks AF, AK, AU, BL, BW, C, C1, CB (doi:10.7914/SN/CB), CH, CM, CN, CU, CZ (doi:10.7914/SN/CZ), DR, FR, G, GE (doi:10.14470/TR560404), GR, GT (doi:10.7914/SN/GT), HU (do:10.14470/UH028726), IC (doi:10.7914/SN/IC), II (doi:10.7914/SN/II), IU (doi:10.7914/SN/IU), IV, IW, KC (doi:10.7914/SN/KC), KN, KR (doi:10.7914/SN/KR), KZ (doi:10.7914/SN/KZ), LD, MN, MS, MY, NA, NL, OE, PL, PM, PR, PS, RM (doi:10.7914/SN/RM), SL, SX, TA (doi:10.7914/SN/TA), TH, TM, US (doi:10.7914/SN/US), X4, X6, XA, XE, XF, XH, XJ, XO (doi:10.7914/SN/XO_1997), XP, XR, XS, XT, XW, YC, YE, YF, YI, YJ, YL, YT, ZB and ZL through the Data Management Center of IRIS, using WILBER II and WILBER III and through the Virtual European Broadband Seismograph Network, run by ORFEUS (http://www.orfeus-eu.org/Data-info/vebsn-contributors.html). The editor, Vernon Cormier, and two anonymous reviewers are thanked for their insights. The author acknowledges the use of GMT [Wessel and Smith, 1998] and TauP [Crotwell et al., 1999] software packages and thanks C. Thomas for her ray tracing software and E.A. Day & A. Valentine for helpful discussions.

Appendix A. Supplementary data

Supplementary data associated with this article can be found, in the online version, at http://dx.doi.org/10.1016/j.pepi.2016.03.001.

References

Al-Khatatbeh, Y., Bergman, M.I., Lewis, D.J., Mason, Z., Zhu, L., Rosenstock, S., 2013. Annealing of directionally solidified alloys revisited: no loss of solidification texture in Earth's inner core. Phys. Earth Planet. Inter. 223, 32–39. http://dx.doi.org/10.1016/j.pepi.2013.04.003.

Alboussière, T., Deguen, R., 2012. Asymmetric dynamics of the inner core and impact on the outer core. J. Geodyn. 61, 172–182. http://dx.doi.org/10.1016/j.jog.2012.07.006.

Alboussiere, T., Deguen, R., Melzani, M., 2010. Melting-induced stratification above the Earth's inner core due to convective translation. Nature 466, 744–747. http://dx.doi.org/10.1038/nature09257.

Aubert, J., Amit, H., Hulot, G., Olson, P., 2008. Thermochemical flows couple the Earth's inner core growth to mantle heterogeneity. Nature 454, 758–761. http://dx.doi.org/10.1038/nature07109.

Beghein, C., Trampert, J., 2003. Robust normal mode constraints on inner-core anisotropy from model space search. Science 299 (5606), 552–555. http://dx.doi.org/10.1126/science.1078159.

Bergman, M.I., 1997. Measurements of elastic anisotropy due to solidification texturing and the implications for the Earth's inner core. Nature 389, 60–63. http://dx.doi.org/10.1038/37962.

Bergman, M.I., 2003. Solidification of the Earth's core. In: Dehant, V., Creager, K.C., Karato, S.-I., Zatman, S. (Eds.), Earth's Core: Dynamics, Structure, Rotation, vol. 31. American Geophysical Union, pp. 105–127. http://dx.doi.org/10.1029/GD031p0105.

Bergman, M.I., Lewis, D.J., Myint, I.H., Slivka, L., Karato, A., Abreu, S.-I., 2010. Grain growth and loss of texture during annealing of alloys, and the translation of earths inner core. Geophys. Res. Lett. 37 (22), L22313. http://dx.doi.org/10.1029/2010GL045103.

Biggin, A.J., Piispa, E.J., Pesonen, L.J., Holme, R., Paterson, G.A., Veikkolainen, T., Tauxe, L., 2015. Palaeomagnetic field intensity variations suggest mesoproterozoic inner-core nucleation. Nature 526 (7572), 245–248. http://dx.doi.org/10.1038/nature15523.

Blom, N.A., Deuss, A., Paulssen, H., Waszek, L., 2015. Inner core structure behind the PKP core phase triplication. Geophys. J. Int. 201 (3), 1657–1665. http://dx.doi.org/10.1093/gji/ggv103.

Bréger, L., Romanowicz, B., Tkalčić, H., 1999. PKP(BC-DF) travel time residuals and short scale heterogeneity in the deep Earth. Geophys. Res. Lett. 26 (20), 3169–3172. http://dx.doi.org/10.1029/1999GL008374.

Bréger, L., Romanowicz, B., Rousset, S., 2000. New constraints on the structure of the inner core from P′P′. Geophys. Res. Lett. 27 (17), 2781–2784. http://dx.doi.org/10.1029/1999GL008467.

Buffett, B.A., 2009. Onset and orientation of convection in the inner core. Geophys. J. Int. 179 (2), 711–719. http://dx.doi.org/10.1111/j.1365-246X.2009.04311.x.

Buffett, B.A., Wenk, H.R., 2001. Texturing of the Earth's inner core by Maxwell stresses. Nature 413 (6851), 60–63. http://dx.doi.org/10.1038/35092543.

Cao, A., Romanowicz, B., 2004. Hemispherical transition of seismic attenuation at the top of the Earth's inner core. Earth Planet. Sci. Lett 228, 243–253. http://dx.doi.org/10.1016/j.epsl.2004.09.032.

Chapman, C.H., 1978. A new method for computing synthetic seismograms. Geophys. J. Int. 54, 481–518. http://dx.doi.org/10.1111/j.1365-246X.1978.tb05491.x.

Chapman, C.H., Orcutt, J.A., 1985. The computation of body wave synthetic seismograms in laterally homogeneous media. Rev. Geophys. 23 (2), 105–163. http://dx.doi.org/10.1029/RG023i002p00105.

Cormier, V.F., Xu, L., Choy, G.L., 1998. Seismic attenuation of the inner core: viscoelastic or stratigraphic? Geophys. Res. Lett. 25 (21), 4019–4022. http://dx.doi.org/10.1029/1998GL900074.

Cottaar, S., Buffett, B., 2012. Convection in the Earth's inner core. Phys. Earth Planet. Inter. 198–199, 67–78. http://dx.doi.org/10.1016/j.pepi.2012.03.008.

Creager, K.C., 1992. Anisotropy of the inner core from differential travel times of the phases PKP and PKIKP. Nature 356 (6367), 309–314. http://dx.doi.org/10.1038/356309a0.

Creager, K.C., 1997. Inner core rotation rate from small-scale heterogeneity and time-varying travel times. Science 278, 1284–1288. http://dx.doi.org/10.1126/science.278.5341.1284.

Creager, K.C., 1999. Large-scale variations in inner core anisotropy. J. Geophys. Res. 104 (B10), 23127–23140. http://dx.doi.org/10.1029/1999JB900162.

Creager, K.C., 2000. Inner core anisotropy and rotation. In: Karato, S.-I., Stixrude, L., Lieberman, R., Masters, G., Forte, A. (Eds.), Earth's Deep Interior: Mineral Physics and Seismic Tomography from the Atomic to the Global Scale, Geophysical Monograph Series, vol. 117. American Geophysical Union, pp. 89–114, http://dx.doi.org/10.1029/GM117p0089.

Davies, C., Pozzo, M., Gubbins, D., Alfè, D., 2015. Constraints from material properties on the dynamics and evolution of Earth's core. Nat. Geosci. 8 (9), 678–685. http://dx.doi.org/10.1038/ngeo2492.

de Koker, N., Steinle-Neumann, G., Vlček, V., 2012. Electrical resistivity and thermal conductivity of liquid Fe alloys at high P and T, and heat flux in Earth's core. Proc. Natl. Acad. Sci. USA 109 (11), 4070–4073. http://dx.doi.org/10.1073/pnas.1111841109.

Deguen, R., Cardin, P., 2011. Thermochemical convection in Earth's inner core. Geophys. J. Int. 187 (3), 1101–1118. http://dx.doi.org/10.1111/j.1365-246X.2011.05222.x.

Deuss, A., Irving, J.C.E., Woodhouse, J.H., 2010. Regional variation of inner core anisotropy from seismic normal mode observations. Science 328 (5981), 1018–1020. http://dx.doi.org/10.1126/science.1188596.

Driscoll, P.E., 2015. Testing the dynamic coupling of the core-mantle and inner core boundaries. J. Geophys. Res. 120 (7), 46894701. http://dx.doi.org/10.1002/2014JB011682.

Durek, J.J., Romanowicz, B., 1999. Inner core anisotropy inferred by direct inversion of normal mode spectra. Geophys. J. Int. 139 (3), 599–622. http://dx.doi.org/10.1046/j.1365-246x.1999.00961.x.

Dziewonski, A.M., Anderson, D., 1981. Preliminary reference earth model. Phys. Earth Planet. Inter. 25 (4), 297–356. http://dx.doi.org/10.1016/0031-9201(81)90046-7.

Dziewonski, A.M., Gilbert, F., 1976. The effect of small, aspherical perturbations on travel times and a re-examination of the corrections for ellipticity. Geophys. J. Roy. Astron. Soc. 44, 7–17. http://dx.doi.org/10.1111/j.1365-246X.1976.tb00271.x.

Dziewonski, A.M., Chou, T.-A., Woodhouse, J.H., 1981. Determination of earthquake source parameters from waveform data for studies of global and regional seismicity. J. Geophys. Res. 86 (B4), 2825–2852. http://dx.doi.org/10.1029/JB086iB04p02825.

Ekström, G., Nettles, M., Dziewonski, A.M., 2012. The global CMT project 2004–2010: centroid-moment tensors for 13,017 earthquakes. Phys. Earth Planet. Inter. 200, 1–9. http://dx.doi.org/10.1016/j.pepi.2012.04.002.

Engdahl, E.R., van der Hilst, R., Buland, R., 1998. Global teleseismic earthquake relocation with improved travel times and procedures for depth determination. Bull. Seismol. Soc. Am. 88 (3), 722–743.

Garcia, R., 2002a. Constrains on upper inner-core structure from waveform inversion of core phases. Geophys. J. Int. 150 (3), 651–664. http://dx.doi.org/10.1046/j.1365-246X.2002.01717.x.

Garcia, R., 2002b. Seismological and mineralogical constraints on the inner core fabric. Geophys. Res. Lett. 29 (20), 1958. http://dx.doi.org/10.1029/2002GL015268.

Garcia, R., Souriau, A., 2000. Inner core anisotropy and heterogeneity level. Geophys. Res. Lett. 27 (19), 3121–3124. http://dx.doi.org/10.1029/2000GL008520.

Garcia, Raphaël, Souriau, Annie, 2001. Correction to inner core anisotropy and heterogeneity level by Raphaël Garcia, and Annie Souriau. Geophys. Res. Lett. 28 (1), 85. http://dx.doi.org/10.1029/2000GL012453.

Geballe, Z.M., Lasbleis, M., Cormier, V.F., Day, E.A., 2013. Sharp hemisphere boundaries in a translating inner core. Geophys. Res. Lett. 40 (9), 1719–1723. http://dx.doi.org/10.1002/grl.50372.

Goldstein, P., Dodge, D., Firpo, M., Minner, L., 2003. SAC2000: signal processing and analysis tools for seismologists and engineers. In: Lee, W.H.K., Kanamori, H., Jennings, P.C., Kisslinger, C. (Eds.), Invited Contribution to the IASPEI International Handbook of Earthquake and Engineering Seismology. Academic Press, London.

Gomi, H., Ohta, K., Hirose, K., Labrosse, S., Caracas, R., Verstraete, M.J., Hernlund, J. W., 2013. The high conductivity of iron and thermal evolution of the Earth's core. Phys. Earth Planet. Inter. 224, 88–103. http://dx.doi.org/10.1016/j.pepi.2013.07.010.

Gubbins, D., Sreenivasan, B., Mound, J., Rost, S., 2011. Melting of the Earth's inner core. Nature 473, 361–363. http://dx.doi.org/10.1038/nature10068.

Irving, J.C.E., Deuss, A., 2011. Hemispherical structure in inner core velocity anisotropy. J. Geophys. Res. 116 (B4), B04307. http://dx.doi.org/10.1029/2010JB007942.

Irving, J.C.E., Deuss, A., 2015. Regional seismic variations in the inner core under the North Pacific. Geophys. J. Int. 203 (3), 2189–2199. http://dx.doi.org/10.1093/gji/ggv435.

Irving, J.C.E., Deuss, A., Andrews, J., 2008. Wide-band coupling of Earth's normal modes due to anisotropic inner core structure. Geophys. J. Int. 174 (3), 919–929. http://dx.doi.org/10.1111/j.1365-246X.2008.03824.x.

Irving, J.C.E., Deuss, A., Woodhouse, J.H., 2009. Normal mode coupling due to hemispherical anisotropic structure in Earth's inner core. Geophys. J. Int. 178 (2), 962–975. http://dx.doi.org/10.1111/j.1365-246X.2009.04211.x.

Ishii, M., Tromp, J., Dziewonski, A.M., Ekstrom, G., 2002a. Joint inversion of normal mode and body wave data for inner core anisotropy 1. Laterally homogeneous anisotropy. J. Geophys. Res. 107 (B12), 2379. http://dx.doi.org/10.1029/2001JB000712.

Ishii, M., Tromp, J., Dziewonski, A.M., Ekstrom, G., 2002b. Joint inversion of normal mode and body wave data for inner core anisotropy 2. Possible complexities. J. Geophys. Res. 107 (B12), 2380. http://dx.doi.org/10.1029/2001JB000713.

Isse, T., Nakanishi, I., 2002. Inner-core anisotropy beneath Australia and differential rotation. Geophys. J. Int. 151 (1), 255–263.

Jeanloz, R., Wenk, H.-R., 1988. Convection and anisotropy of the inner core. Geophys. Res. Lett. 15 (1), 72–75. http://dx.doi.org/10.1029/GL015i001p00072.

Karato, S.I., 1993. Inner core anisotropy due to the magnetic field-induced preferred orientation of iron. Science 262 (5140), 1708–1711. http://dx.doi.org/10.1126/science.262.5140.1708.

Karato, S.I., 1999. Seismic anisotropy of the Earth's inner core resulting from flow induced by Maxwell stresses. Nature 402 (6764), 871–873. http://dx.doi.org/10.1038/47235.

Kennett, B.L.N., Engdahl, E.R., 1991. Traveltimes for global earthquake location and phase identification. Geophys. J. Int. 105 (2), 429–465. http://dx.doi.org/10.1111/j.1365-246X.1991.tb06724.x.

Kennett, B.L.N., Gudmundsson, O., 1996. Ellipticity corrections for seismic phases. Geophys. J. Int. 127 (1), 40–48. http://dx.doi.org/10.1111/j.1365-246X.1996.tb01533.x.

Kennett, B.L.N., Engdahl, E.R., Buland, R., 1995. Constraints on seismic velocities in the Earth from travel times. Geophys. J. Int. 122 (1), 108–124. http://dx.doi.org/10.1111/j.1365-246X.1995.tb03540.x.

Labrosse, S., 2015. Thermal evolution of the core with a high thermal conductivity. Phys. Earth Planet. Inter. 247, 36–55. http://dx.doi.org/10.1016/j.pepi.2015.02.002.

Labrosse, S., Poirier, J.-P., Le Mouël, J.-L., 2001. The age of the inner core. Earth Planet. Sci. Lett 190, 111–123. http://dx.doi.org/10.1016/S0012-821X(01)00387-9.

Lasbleis, M., Deguen, R., 2015. Building a regime diagram for the Earth's inner core. Phys. Earth Planet. Inter. 247, 80–93. http://dx.doi.org/10.1016/j.pepi.2015.02.001.

Leykam, D., Tkalčić, H., Reading, A.M., 2010. Core structure re-examined using new teleseismic data recorded in Antarctica: evidence for, at most, weak cylindrical seismic anisotropy in the inner core. Geophys. J. Int. 180 (3), 1329–1343. http://dx.doi.org/10.1111/j.1365-246X.2010.04488.x.

Li, A., Richards, P.G., 2003. Study of inner core structure and rotation using seismic records from Novaya Zemlya underground nuclear tests. In: Dehant, V., Creager, K.C., Karato, S.-I., Zatman, S. (Eds.), Earth's Core: Dynamics, Structure, Rotation, vol. 31. American Geophysical Union, pp. 23–30, http://dx.doi.org/10.1029/GD031p0023.

Lythgoe, K.H., Deuss, A., Rudge, J.F., Neufeld, J.A., 2014. Earth's inner core: innermost inner core or hemispherical variations? Earth Planet. Sci. Lett 385, 181–189. http://dx.doi.org/10.1016/j.epsl.2013.10.049.

Mäkinen, A.M., Deuss, A., 2011. Global seismic body-wave observations of temporal variations in the Earth's inner core, and implications for its differential rotation. Geophys. J. Int. 187, 355–370. http://dx.doi.org/10.1111/j.1365-246X.2011.05146.x.

Miller, M.S., Niu, F., Vanacore, E.A., 2013. Aspherical structural heterogeneity within the uppermost inner core: Insights into the hemispherical boundaries and core formation. Phys. Earth Planet. Inter. 223, 8–20. http://dx.doi.org/10.1016/j.pepi.2013.02.001.

Mizzon, H., Monnereau, M., 2013. Implication of the lopsided growth for the viscosity of Earth's inner core. Earth Planet. Sci. Lett 361, 391–401. http://dx.doi.org/10.1016/j.epsl.2012.11.005.

Monnereau, M., Calvet, M., Margerin, L., Souriau, A., 2010. Lopsided growth of Earth's inner core. Science 328, 1014–1017. http://dx.doi.org/10.1126/science.1186212.

Morelli, A., Dziewonski, A.M., Woodhouse, J.H., 1986. Anisotropy of the inner core inferred from PKIKP travel times. Geophys. Res. Lett. 13 (13), 1545–1548. http://dx.doi.org/10.1029/GL013i013p01545.

Niu, F., Wen, L., 2001. Hemispherical variations in seismic velocity at the top of the Earth's inner core. Nature 410 (6832), 1081–1084. http://dx.doi.org/10.1038/35074073.

Ohtaki, T., Kaneshima, S., Kanjo, K., 2012. Seismic structure near the inner core boundary in the south polar region. J. Geophys. Res. 117 (B3). http://dx.doi.org/10.1029/2011JB008717.

Olson, P., 2013. The new core paradox. Science 342 (6157), 431–432. http://dx.doi.org/10.1126/science.1243477.

Oreshin, S.I., Vinnik, L.P., 2004. Heterogeneity and anisotropy of seismic attenuation in the inner core. Geophys. Res. Lett. 31 (2), 2613. http://dx.doi.org/10.1029/2003GL018591.

Ovtchinnikov, V.M., Kaazik, P.B., Krasnoshchekov, D.N., 2012. Weak velocity anomaly in the Earth's outer core from seismic data. Izvestia Phys. Solid Earth 48 (3), 211–221. http://dx.doi.org/10.1134/S1069351312020036.

Pozzo, M., Davies, C., Gubbins, D., Alfè, D., 2012. Thermal and electrical conductivity of iron at Earth's core conditions. Nature 485 (7398), 355–358. http://dx.doi.org/10.1038/nature11031.

Romanowicz, B., Li, X.D., Durek, J., 1996. Anisotropy in the inner core: could it be due to low-order convection? Science 274 (5289), 963–966. http://dx.doi.org/10.1126/science.274.5289.963.

Romanowicz, B., Tkalčič, H., Bréger, L., 2003. On the origin of complexity in PKP travel time data. In: Dehant, V., Creager, K.C., Karato, S.-I., Zatman, S. (Eds.), Earth's Core: Dynamics, Structure, Rotation. American Geophysical Union, pp. 31–44, http://dx.doi.org/10.1029/GD031p0031.

Shearer, P.M., 1994. Constraints on inner core anisotropy from PKP(df) travel times. J. Geophys. Res. 99 (B10), 19647–19659. http://dx.doi.org/10.1029/94JB01470.

Shearer, P.M., Toy, K.M., 1991. PKP(BC) versus PKP(DF) differential travel times and aspherical structure in the Earth's inner core. J. Geophys. Res. 96 (B2), 2233–2247. http://dx.doi.org/10.1029/90JB02370.

Shearer, P.M., Toy, K.M., Orcutt, J.A., 1988. Axi-symmetric Earth models and inner-core anisotropy. Nature 333, 228–232. http://dx.doi.org/10.1038/333228a0.

Singh, S.C., Taylor, M.A.J., Montagner, J.P., 2000. On the presence of liquid in Earth's inner core. Science 287 (5462), 2471–2474. http://dx.doi.org/10.1126/science.287.5462.2471.

Smirnov, A.V., Tarduno, J.A., 2004. Secular variation of the late archean – early proterozoic geodynamo. Geophys. Res. Lett. 31 (16), L16607. http://dx.doi.org/10.1029/2004GL020333.

Song, X., Helmberger, D.V., 1993. Anisotropy of the Earth's inner core. Geophys. Res. Lett. 20 (23), 2591–2594. http://dx.doi.org/10.1029/93GL02812.

Song, X., Helmberger, D.V., 1995. Depth dependence of anisotropy of Earth's inner core. J. Geophys. Res. 100 (B6), 9805–9816. http://dx.doi.org/10.1029/95JB00244.

Song, X., Helmberger, D.V., 1998. Seismic evidence for an inner core transition zone. Science 282 (5390), 924–927. http://dx.doi.org/10.1126/science.282.5390.924.

Song, X., Richards, P.G., 1996. Seismological evidence for differential rotation of the Earth's inner core. Nature 382 (6588), 221–224. http://dx.doi.org/10.1038/382221a0.

Song, X., Xu, X., 2002. Inner core transition zone and anomalous PKP(DF) waveforms from polar paths. Geophys. Res. Lett. 29 (4), 1. http://dx.doi.org/10.1029/2001GL013822.

Souriau, A., Poupinet, G., 2003. Inner core rotation: a critical appraisal. In: Dehant, V., Creager, K.C., Karato, S.-I., Zatman, S. (Eds.), Earth's Core: Dynamics, Structure, Rotation, vol. 31. American Geophysical Union, pp. 65–82, http://dx.doi.org/10.1029/GD031p0065.

Souriau, A., Romanowicz, B., 1996. Anisotropy in inner core attenuation: a new type of data to constrain the nature of the solid core. Geophys. Res. Lett. 23 (1), 1–4. http://dx.doi.org/10.1029/95GL03583.

Sreenivasan, B., Gubbins, D., 2011. On mantle-induced heat flow variations at the inner core boundary. Phys. Earth Planet. Inter. 187 (3), 336–341. http://dx.doi.org/10.1016/j.pepi.2011.06.006.

Sumita, I., 2007. Thermal coupling between the mantle, outer core and inner core: an experimental model. EOS Trans. AGU Fall Meet. Suppl. 88 (52), DI24A-02.

Sumita, I., Olson, P., 1999. A laboratory model for convection in Earth's core driven by a thermally heterogeneous mantle. Science 286 (5444), 1547–1549. http://dx.doi.org/10.1126/science.286.5444.1547.

Sun, X., Song, X., 2008. Tomographic inversion for three-dimensional anisotropy of Earth's inner core. Phys. Earth Planet. Inter. 167, 53–70. http://dx.doi.org/10.1016/j.pepi.2008.02.011.

Tanaka, S., 2012. Depth extent of hemispherical inner core from PKP(DF) and PKP (Cdiff) for equatorial paths. Phys. Earth Planet. Inter. 210, 50–62. http://dx.doi.org/10.1016/j.pepi.2012.08.001.

Tanaka, S., Hamaguchi, H., 1997. Degree one heterogeneity and hemispherical variation of anisotropy in the inner core from PKP(BC)–PKP(DF) times. J. Geophys. Res. 102 (B2), 2925–2938. http://dx.doi.org/10.1029/96JB03187.

Tarduno, J.A., Cottrell, R.D., Davis, W.J., Nimmo, F., Bono, R.K., 2015. A Hadean to Paleoarchean geodynamo recorded by single zircon crystals. Science 349 (6247), 521–524. http://dx.doi.org/10.1126/science.aaa9114.

Tkalčić, H., 2010. Large variations in travel times of mantle-sensitive seismic waves from the South Sandwich Islands: is the Earth's inner core a conglomerate of anisotropic domains? Geophys. Res. Lett. 37 (14), 14312. http://dx.doi.org/10.1029/2010GL043841.

Torsvik, T.H., Burke, K., Steinberger, B., Webb, S.J., Ashwal, L.D., 2010. Diamonds sampled by plumes from the core-mantle boundary. Nature 466, 352–355. http://dx.doi.org/10.1038/nature09216.

Tromp, J., 1993. Support for anisotropy of the Earth's inner core from free oscillations. Nature 366 (6456), 678–681. http://dx.doi.org/10.1038/366678a0.

Waszek, L., Deuss, A., 2011. Distinct layering in the hemispherical seismic velocity structure of Earth's upper inner core. J. Geophys. Res. 116 (B12), B12313. http://dx.doi.org/10.1029/2011JB008650.

Waszek, L., Irving, J.C.E., Deuss, A., 2011. Reconciling the hemispherical structure of Earth's inner core with its super-rotation. Nat. Geosci. 4 (4), 264–267. http://dx.doi.org/10.1038/ngeo1083.

Wen, L., Niu, F., 2002. Seismic velocity and attenuation structures in the top of the Earth's inner core. J. Geophys. Res. 107 (B11), 2273. http://dx.doi.org/10.1029/2001JB000170.

Wenk, H.R., Takeshita, T., Jeanloz, R., C Johnson, G., 1988. Development of texture and elastic anisotropy during deformation of hcp metals. Geophys. Res. Lett. 15 (1), 76–79. http://dx.doi.org/10.1029/GL015i001p00076.

Woodhouse, J.H., Giardini, D., Li, X.-D., 1986. Evidence for inner core anisotropy from free oscillations. Geophys. Res. Lett. 13 (13), 1549–1552. http://dx.doi.org/10.1029/GL013i013p01549.

Yoshida, S., Sumita, I., Kumazawa, M., 1998. Models of the anisotropy of the Earth's inner core. J. Phys.: Condens. Matter 10, 11215–11226. http://dx.doi.org/10.1088/0953-8984/10/49/011.

Yoshida, S.I., Sumita, I., Kumazawa, M., 1996. Growth model of the inner core coupled with the outer core dynamics and the resulting elastic anisotropy. J. Geophys. Res. 101, 28085. http://dx.doi.org/10.1029/96JB02700.

Yu, J., Bergman, M.I., Huguet, L., Alboussiere, T., 2015. Partial melting of a Pb-Sn mushy layer due to heating from above, and implications for regional melting of Earth's directionally solidified inner core. Geophys. Res. Lett. 42, 064908. http://dx.doi.org/10.1002/2015GL064908.

Yu, W., 2016. Time-dependent inner core structures examined using repeating earthquakes in subduction zones of the southwest pacific. J. Geophys. Res. 204 (2), 1204–1215. http://dx.doi.org/10.1093/gji/ggv508.

Yu, W., Wen, L., 2006a. Seismic velocity and attenuation structures in the top 400 km of the Earth's inner core along equatorial paths. J. Geophys. Res. 111, 7308. http://dx.doi.org/10.1029/2005JB003995.

Yu, W., Wen, L., 2006b. Inner core attenuation anisotropy. Earth Planet. Sci. Lett 245, 581–594. http://dx.doi.org/10.1016/j.epsl.2006.03.043.

Yu, W., Wen, L., 2007. Complex seismic anisotropy in the top of the Earth's inner core beneath Africa. J. Geophys. Res. 112 (B8), 8304. http://dx.doi.org/10.1029/2006JB004868.

Yu, W., Wen, L., Niu, F., 2005. Seismic velocity structure in the Earth's outer core. J. Geophys. Res. 110. http://dx.doi.org/10.1029/2003JB002928.

Zhang, P., Cohen, R.E., Haule, K., 2015. Effects of electron correlations on transport properties of iron at Earth's core conditions. Nature 517 (7536), 605–607. http://dx.doi.org/10.1038/nature14090.